*Supplement of:*

# Extreme ozone episodes in a major Mediterranean urban area

Jordi Massagué[1,2], Eduardo Torre-Pascual[3], Cristina Carnerero[1,4,*], Miguel Escudero[5], Andrés Alastuey[1], Marco Pandolfi[1], Xavier Querol[1], Gotzon Gangoiti[3]

[1]Institute of Environmental Assessment and Water Research (IDAEA-CSIC), Barcelona, 08034, Spain
[2]Department of Mining, Industrial and ICT Engineering, Universitat Politècnica de Catalunya-BarcelonaTech, (UPC), Manresa, 08242, Spain
[3]Faculty of Engineering Bilbao. University of the Basque Country (UPV/EHU), Bilbao, 48013, Spain
[4]Department of Civil and Environmental Engineering, Universitat Politècnica de Catalunya-BarcelonaTech, (UPC), Barcelona, 08034, Spain
[5]Department of Applied Physics. School of Engineering and Architecture. Universidad de Zaragoza (UNIZAR), Zaragoza, 50018, Spain
*Current affiliation: Barcelona Supercomputing Center, Barcelona, 08034, Spain

*Correspondence to:* Jordi Massagué (jordi.massague@idaea.csic.es)

*Contents*

## S1. 2015 episode (6 June)
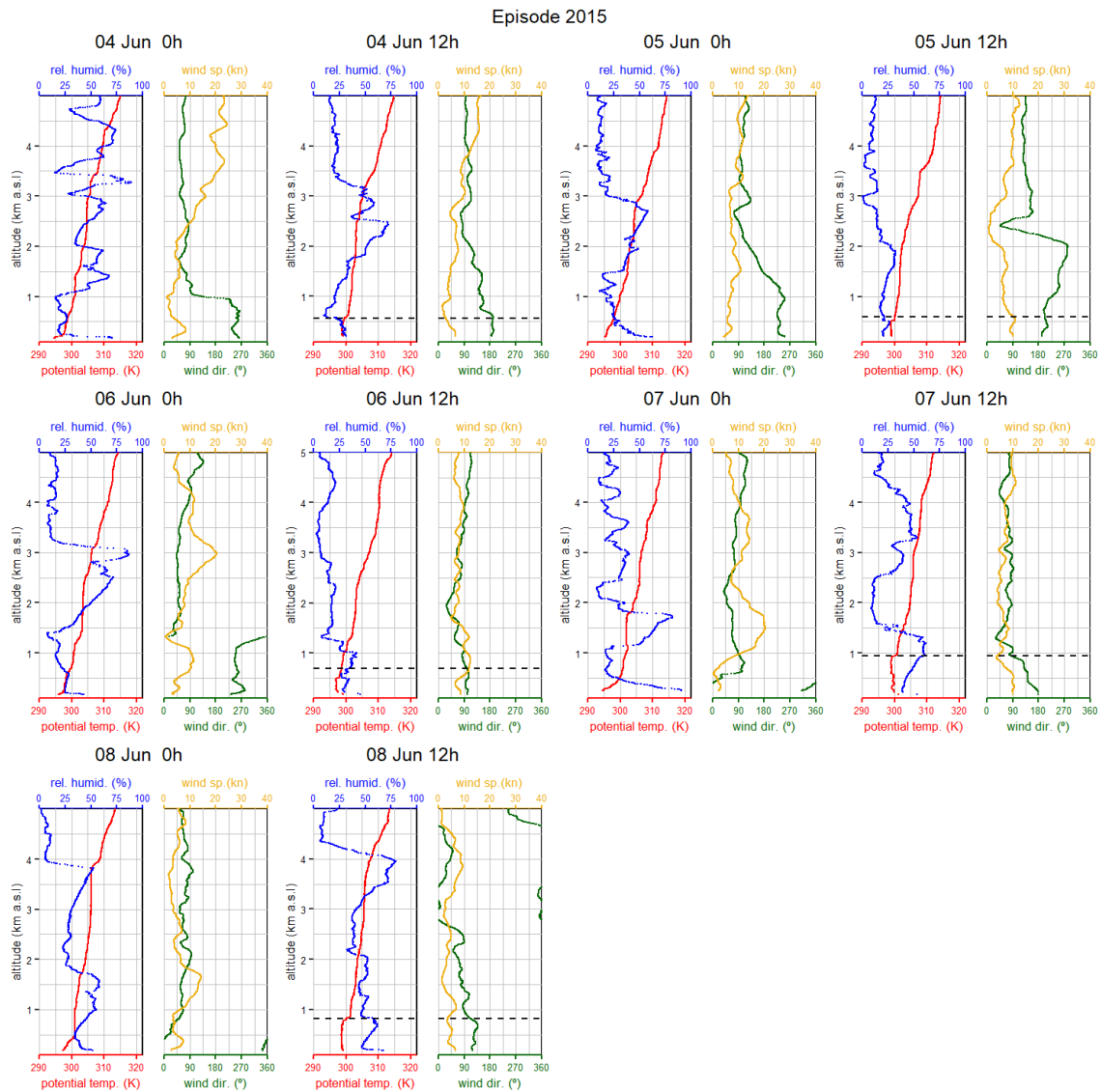
Figure S1.1. Radiosonde data (2015 episode). Midnight and midday potential temperature, relative humidity, wind direction and speed in Barcelona (0–5,000 m above sea level). Horizontal dotted lines represent mixing layer height (MLH). MLHs are shown for noon data.
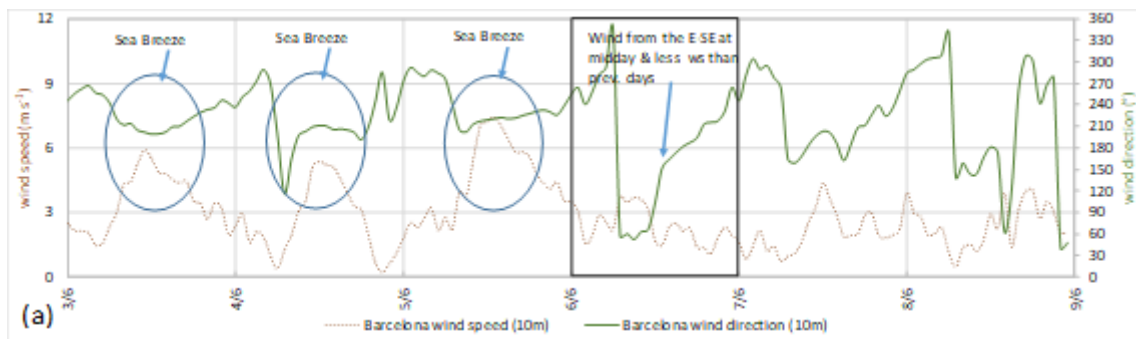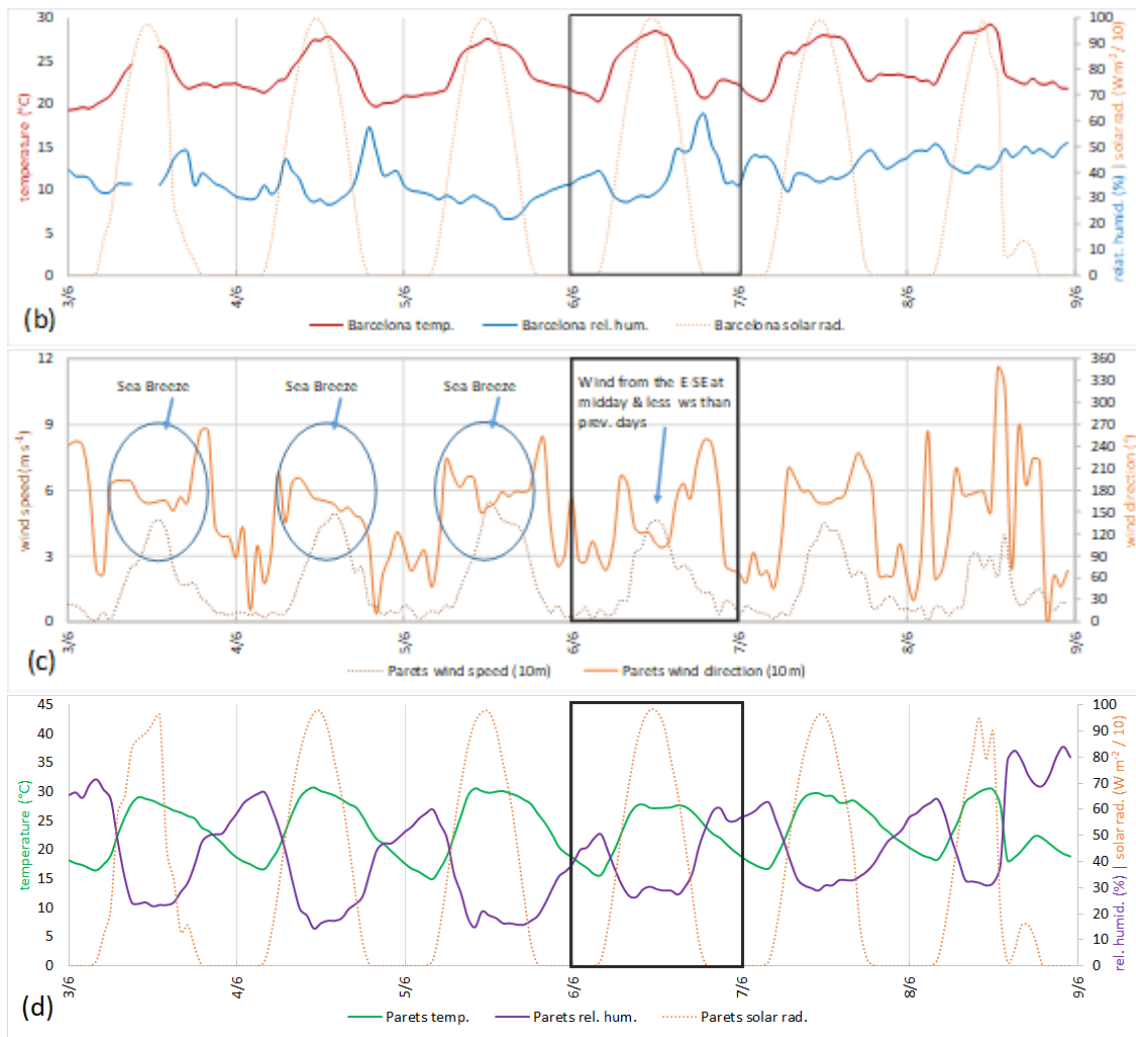
*Figure S1.2. Surface meteorological parameters (2015 episode). (a): Barcelona wind speed and direction (10 m above ground level (AGL)). (b) Barcelona temperature, relative humidity, solar radiation, (c) Parets (25 km northward, downwind of Barcelona) wind speed and direction (10 m AGL) and (d) Parets temperature, relative humidity, solar radiation.*
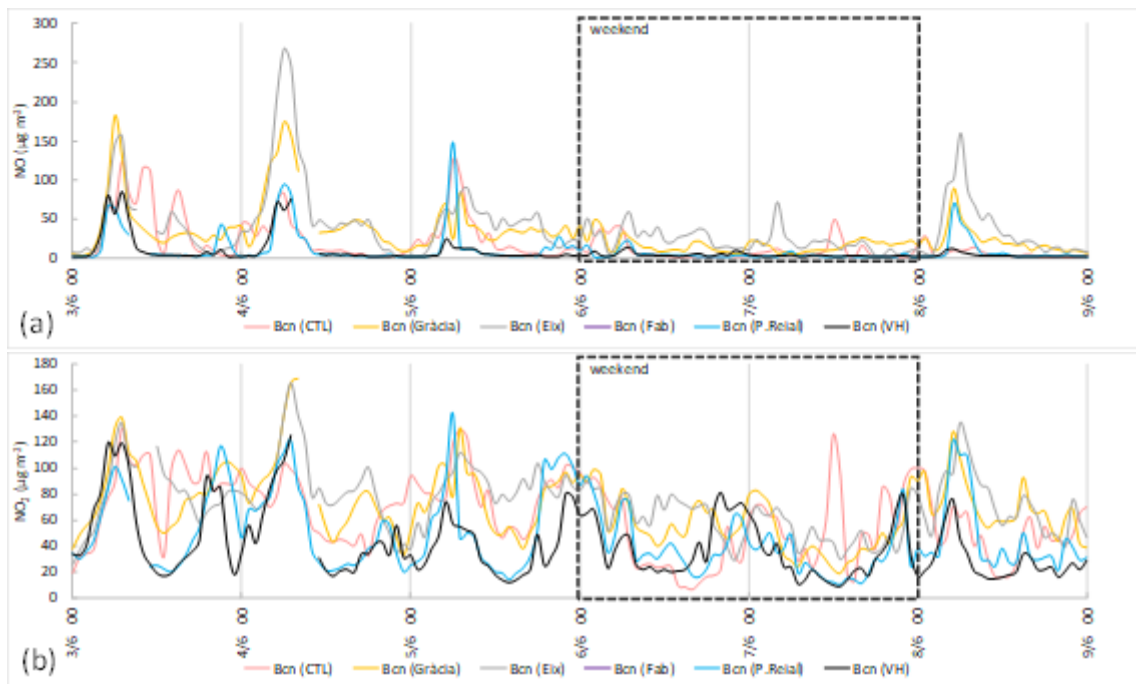
*Figure S1.3. (a) NO and (b) NO₂ concentrations observed in Barcelona during the 2015 episode. A reduction in the NOx concentrations is evident during the weekend.*
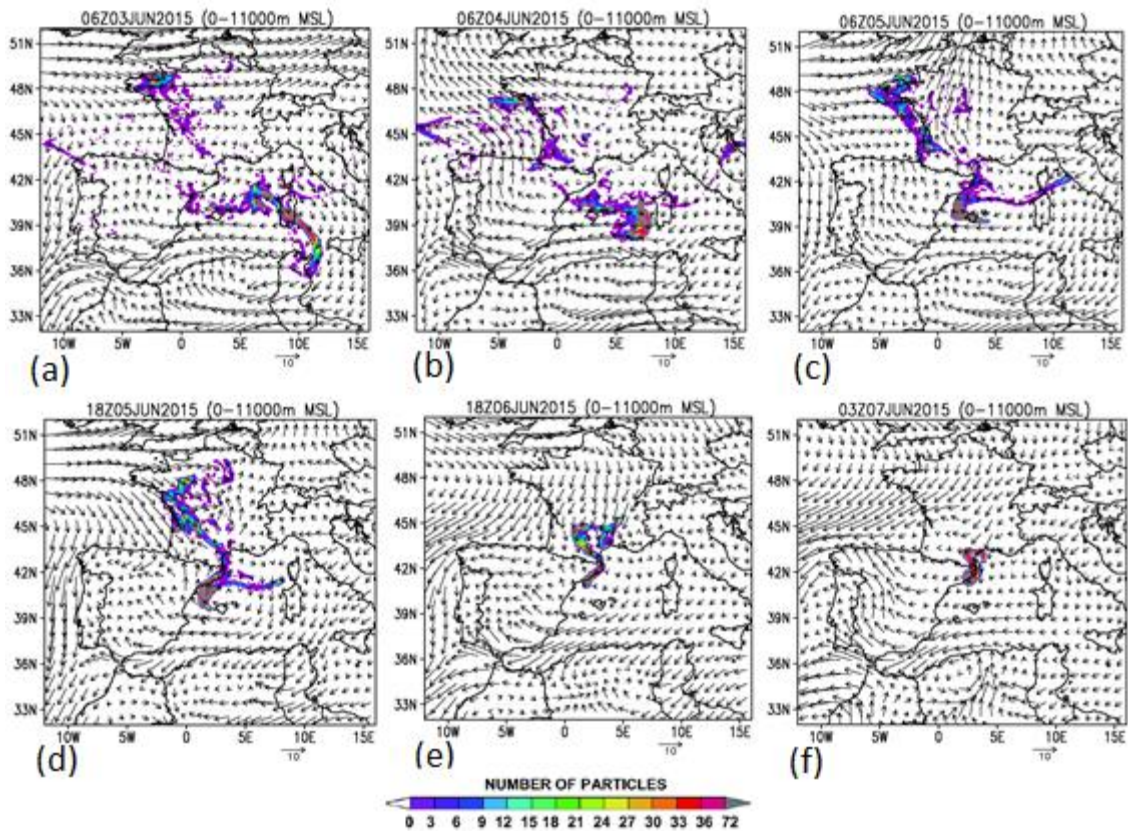
*Figure S1.4. Episode 2015. RAMS/HYPACT back-trajectories of arrival in Barcelona (Ciutadella) the 6 (day of episode) and 7 June. Vectors are average wind from 0–1,000 m AGL (sigma levels), and the shaded areas represent the total number of particles accumulated on the vertical of the site. (a–d) crossing the Western Mediterranean with east and southeast winds during June 3–5, and from France with west winds on the 5 June (e,f) From the South, along the East coast of Spain (Mediterranean influence) with the Mediterranean Gyre circulation, and from the North, through the Gulf of Lyon, sweeping the South of France.*
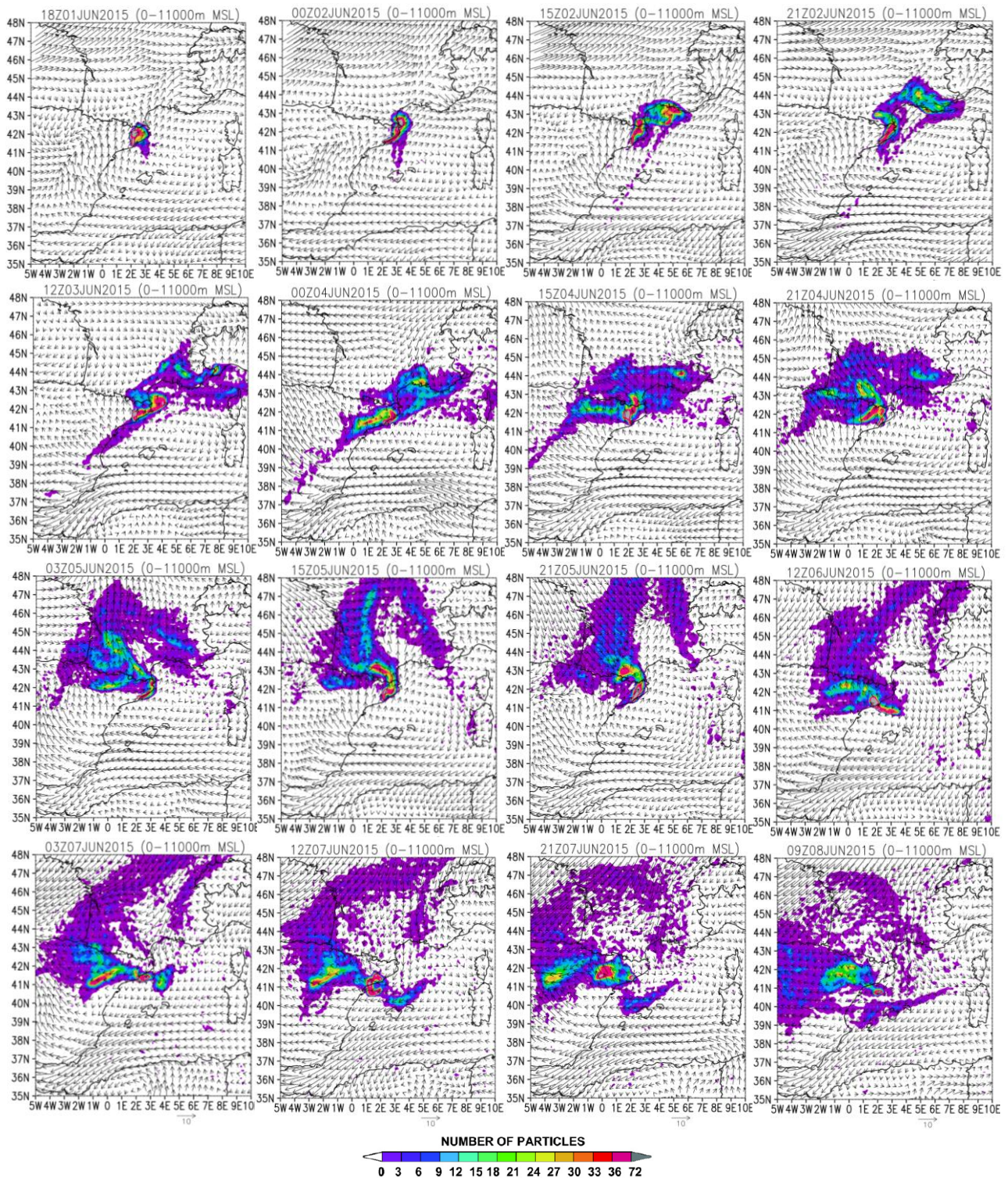
*Figure S1.5. Dispersion sequence of the Barcelona plume (emitted from the centre of the city) along with the average wind field at 0–800 m AGL, which explains the transport pattern. Before June 6, the transport is directed northward, and there is no recirculation (sea-land) of the emissions. On and after June 6 (coinciding with the Tramontana winds), there is sea-land recirculation along the Barcelona coast. The plume completes a full rotation every day, and Barcelona is situated at the centre of a convergence zone for airflows coming from the Gulf of Lion. These airflows move southward parallel to the coast during the night and merge with the emissions from the south and southeast, influenced by sea breezes and the Mediterranean circulation.*
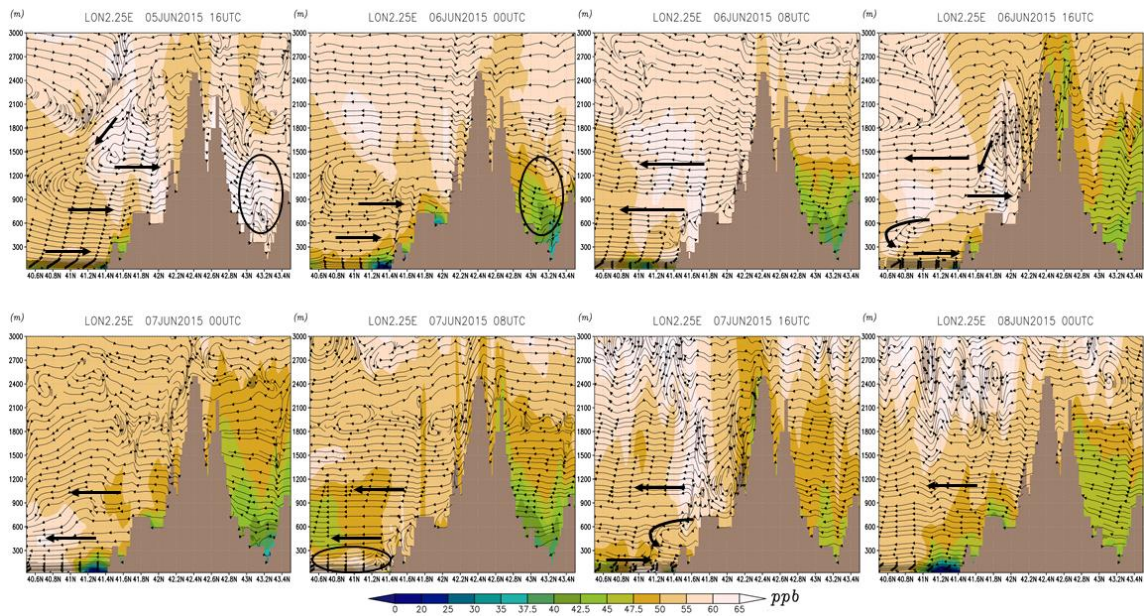
*Figure S1.6. Episode 2015. Simulated O₃ along the cross section Barcelona-Vic. Horizontal winds projected together with vertical wind.s*

## S2. 2018 episode (4 and 5 August)
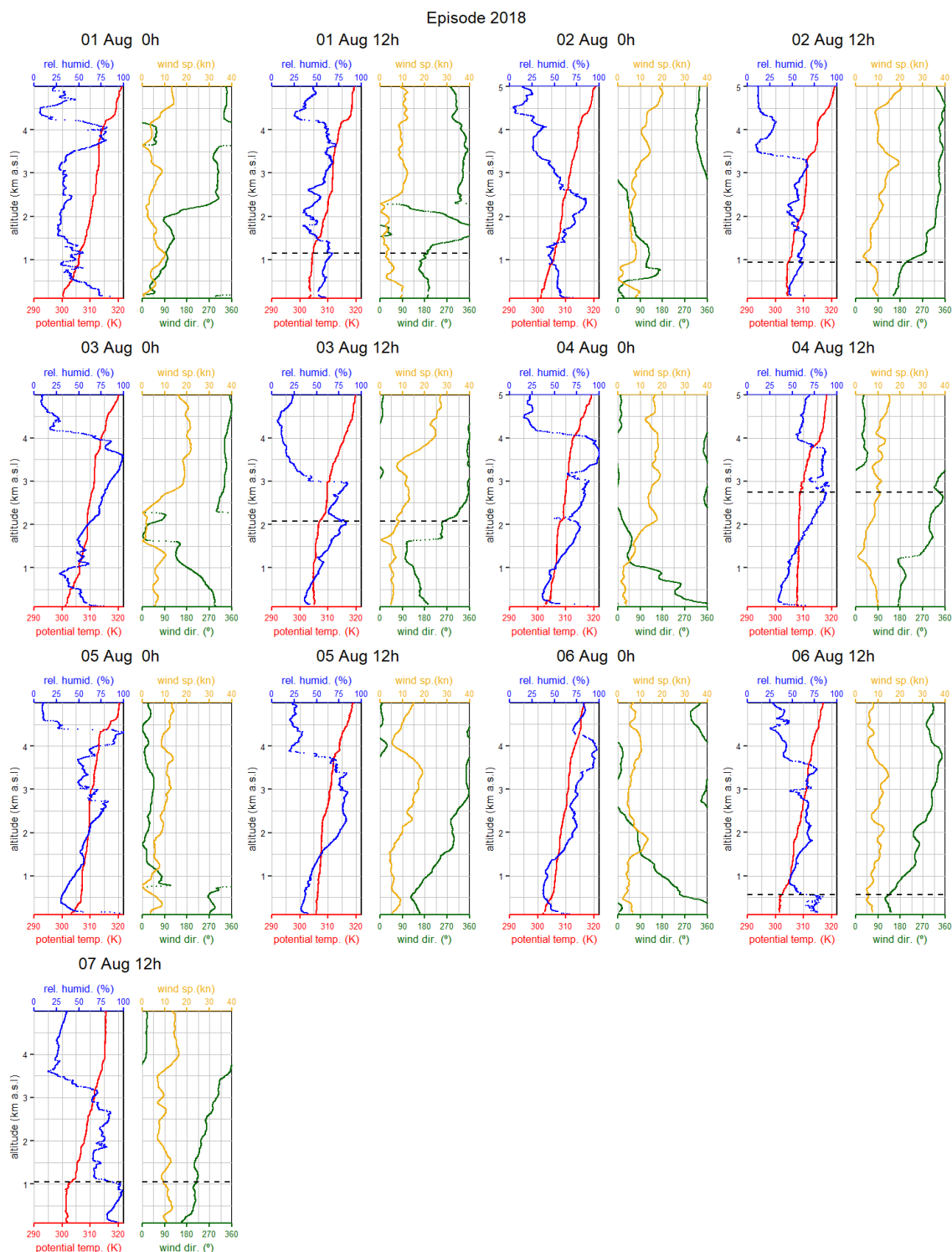
*Figure S2.1. Radiosonde data (2018 episode). Midnight and midday potential temperature, relative humidity, wind direction and speed in Barcelona for 0–5,000 m above sea level.. Horizontal dotted lines represent mixing layer height (MLH). MLHs are shown for noon data with some missing due to technical issues. No radiosonde data for the night of the 7 August.*
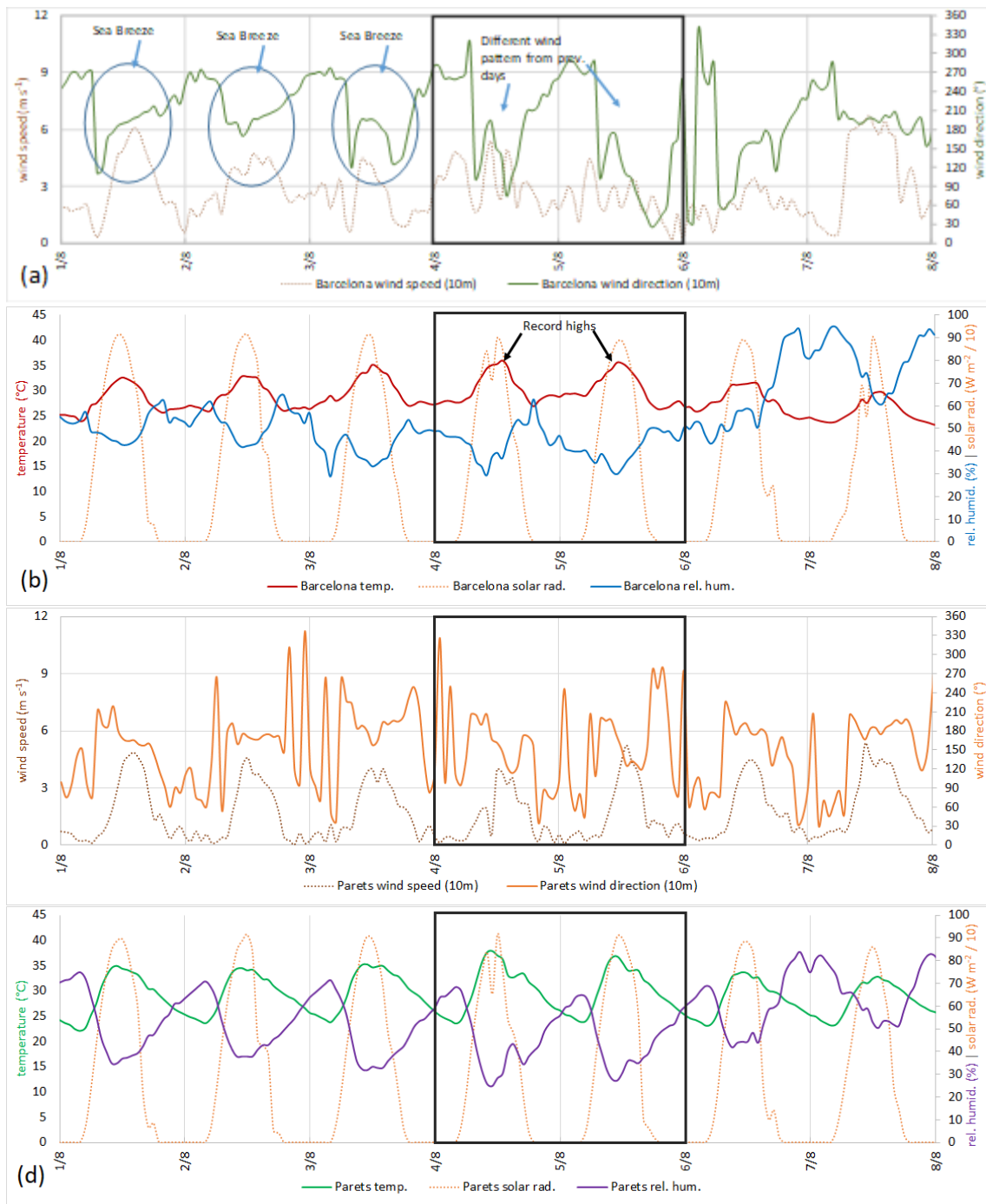
Figure S2.2. Surface meteorological parameters (2018 episode). (a): Barcelona wind speed and direction (10 m above ground level (AGL)). (b) Barcelona temperature, relative humidity, solar radiation and (c) Parets (25 km downwind of Barcelona) wind speed and direction (10 m AGL) and (d) Parets temperature, relative humidity, solar radiation.
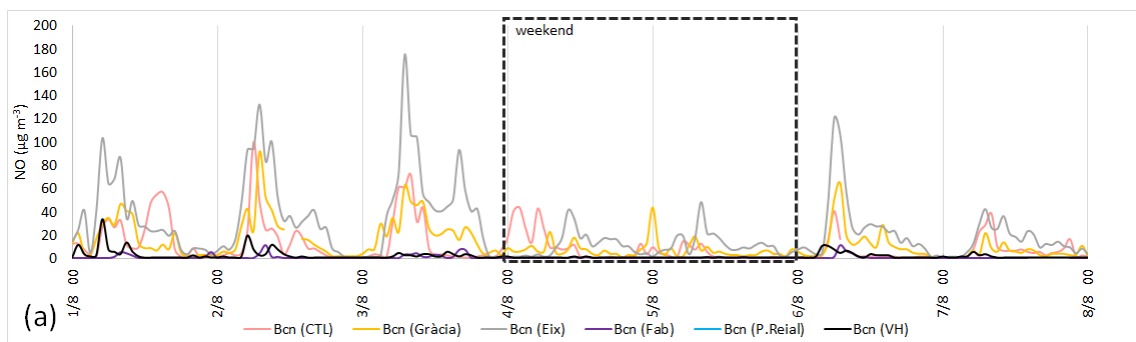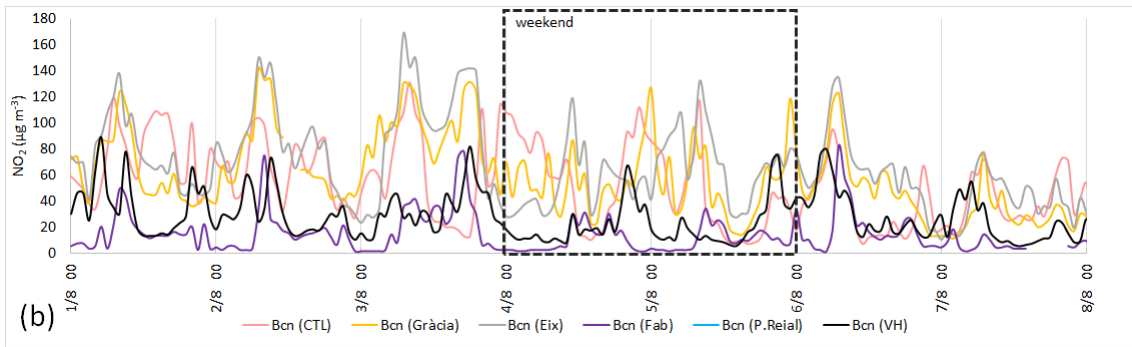
*Figure S2.3. (a) NO and (b) NO₂ concentrations observed in Barcelona during the 2018 episode. A reduction in the NOx concentrations is evident during the weekend.*
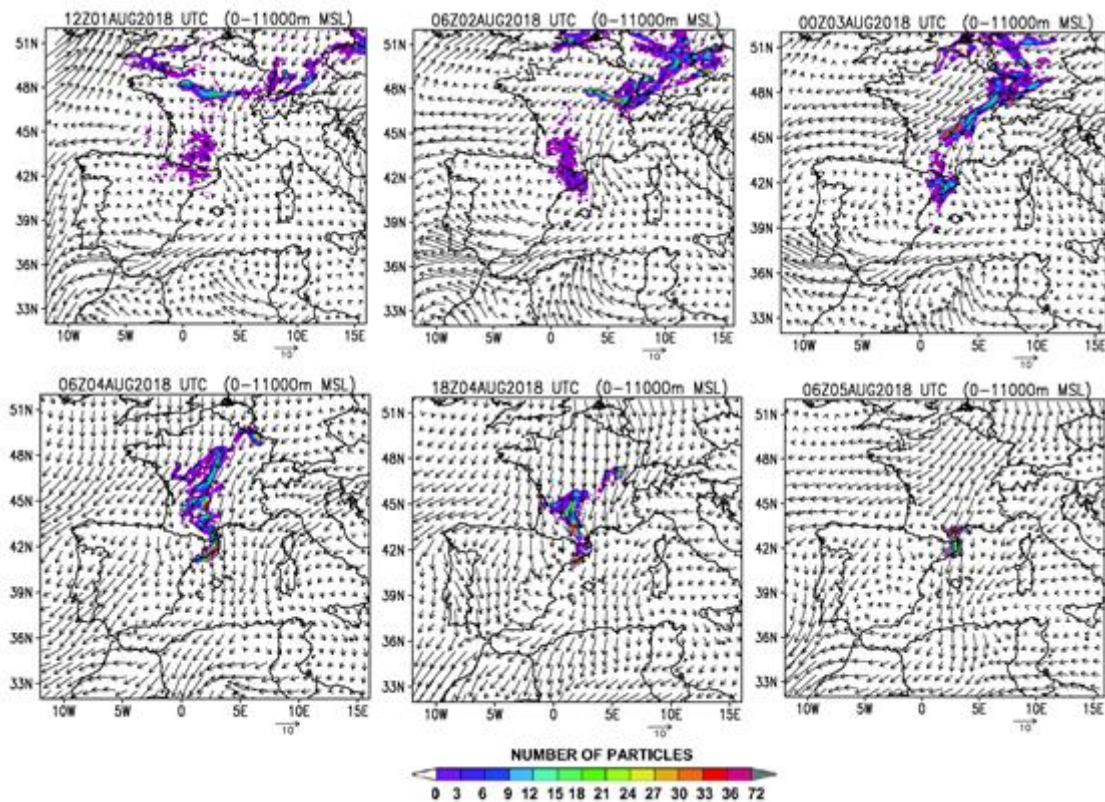
*Figure S2.4. Episode 2018. RAMS/HYPACT back-trajectories of arrival in Barcelona (Fabra) the 4 and 5 of August 2018 (days of episode). Vectors are average wind from 0–1,000 m AGL (sigma levels), and the shaded areas represent the total number of particles accumulated on the vertical of the site. Top row, before the episode, bottom row during the episode.*
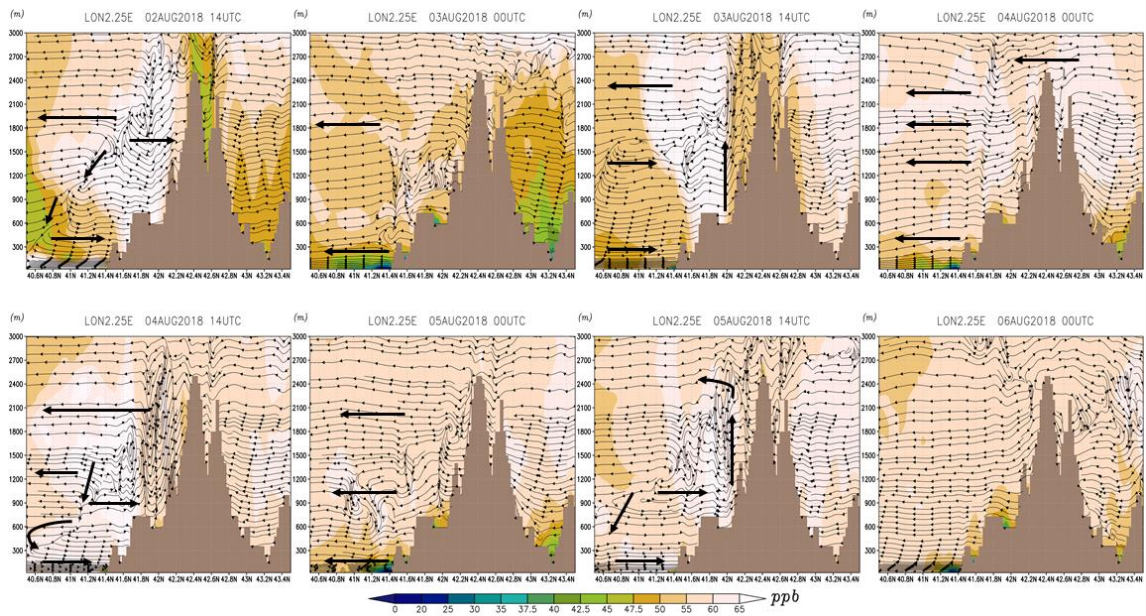
*Figure S2.5. Episode 2018. Simulated O₃ along the cross section Barcelona-Vic. Horizontal winds projected together with vertical winds.*

## S3. 2019 episode (29 June)
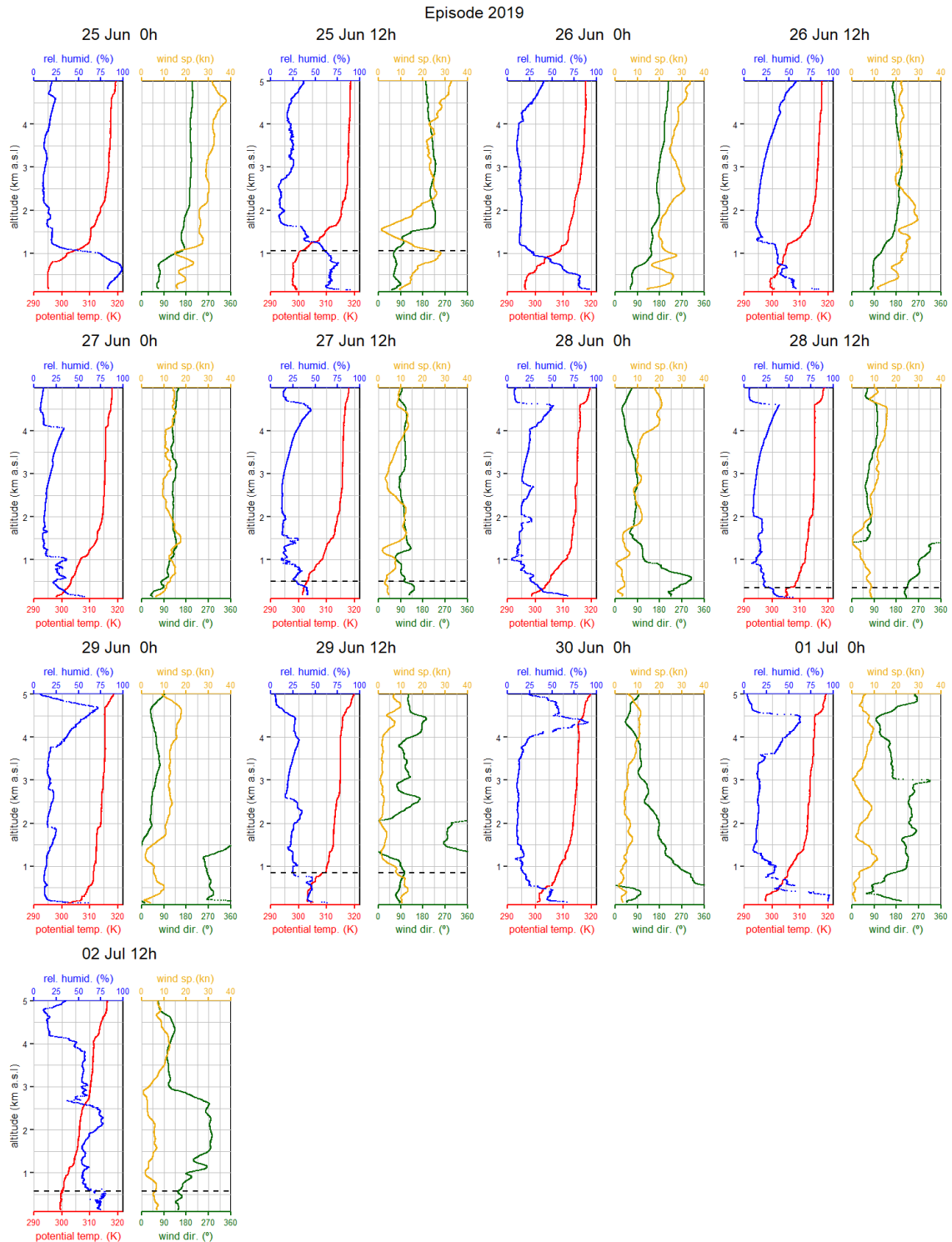
*Figure S3.1. Radiosonde data (2019 episode). Midnight and midday potential temperature, relative humidity, wind direction and speed in Barcelona for 0–5,000 m above sea level. Horizontal dotted lines represent mixing layer height (MLH). MLHs are shown for noon data, some missing due to technical issues. No radiosonde data for the midday of 30 June, 1 July, and for the night of the 2 July.*
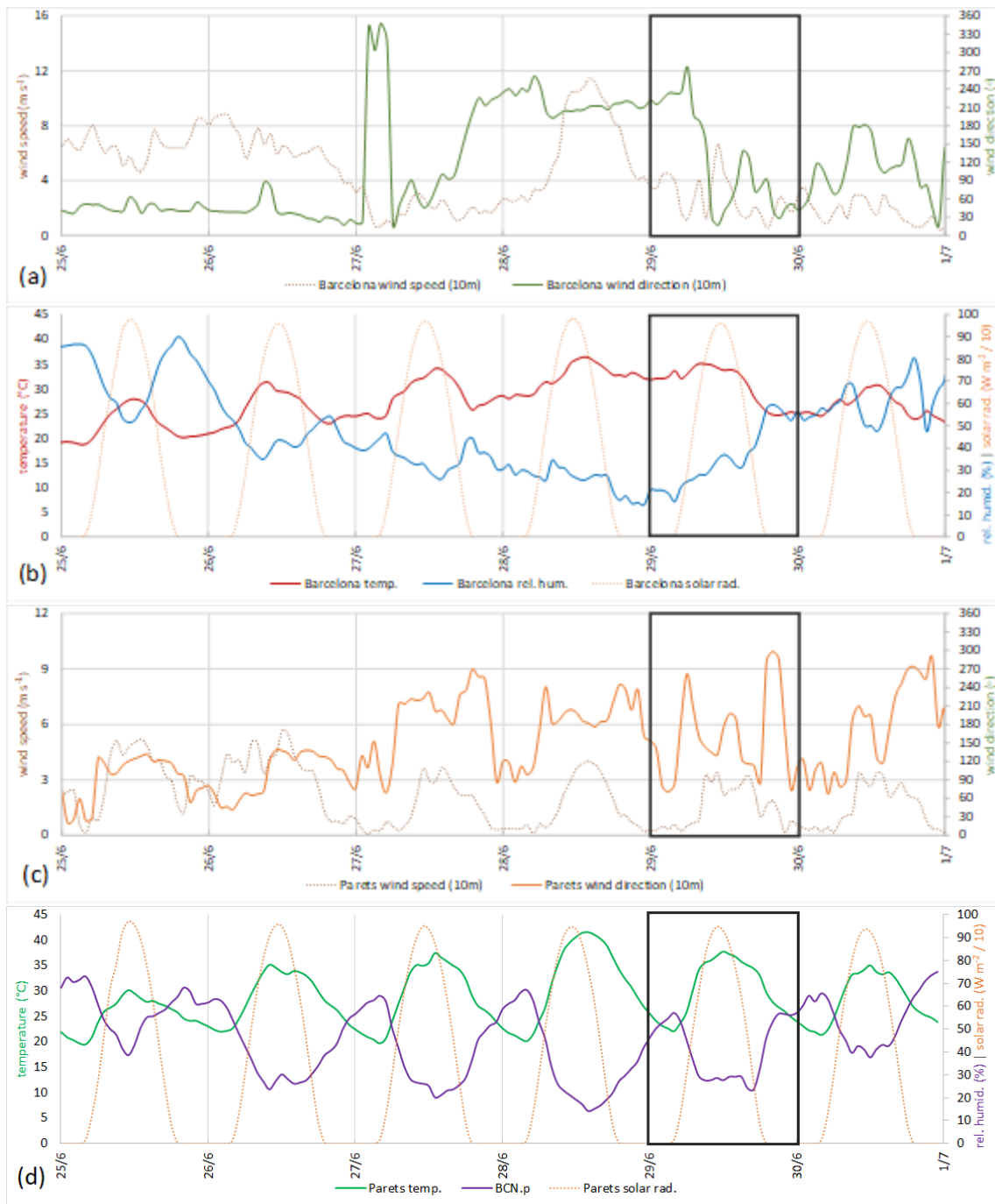
*Figure S3.2. Surface meteorological parameters during (2019 episode). (a): Barcelona wind speed and direction (10 m above ground level (AGL)). (b) Barcelona temperature, relative humidity, solar radiation, (c) Parets (25 km northward, downwind of Barcelona) wind speed and direction (10 m AGL) and (d) Parets temperature, relative humidity, solar radiation.*
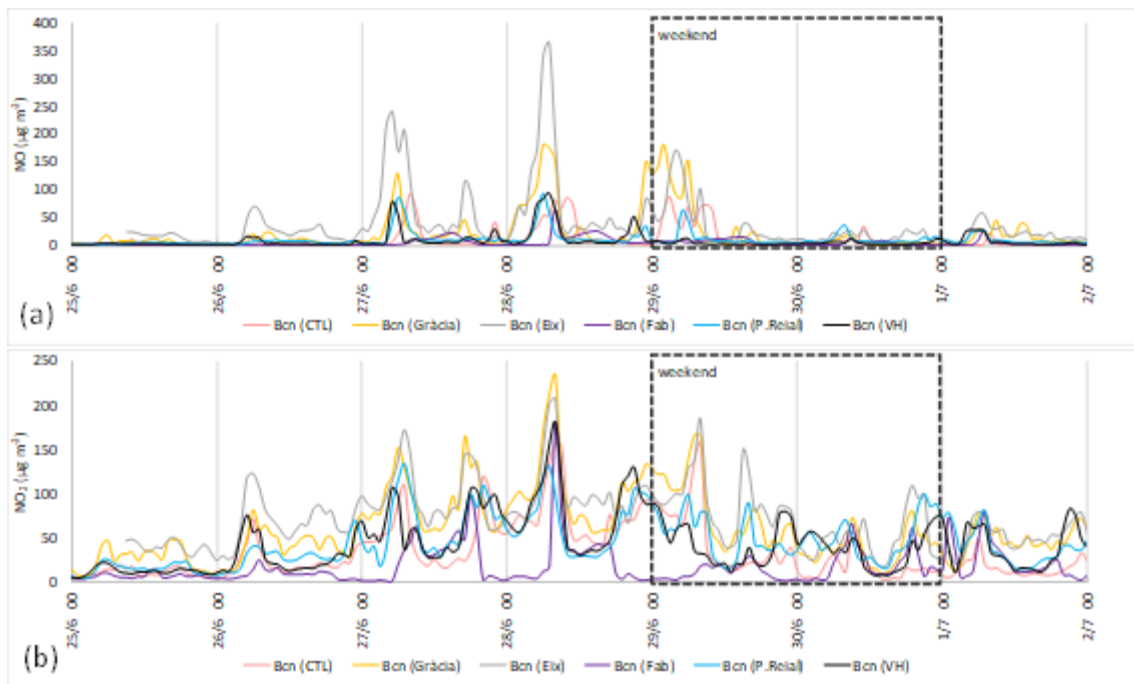
*Figure S3.3. (a) NO and (b) NO₂ concentrations observed in Barcelona during the 2019 episode. A reduction in the NOx concentrations can be observed on the weekend.*
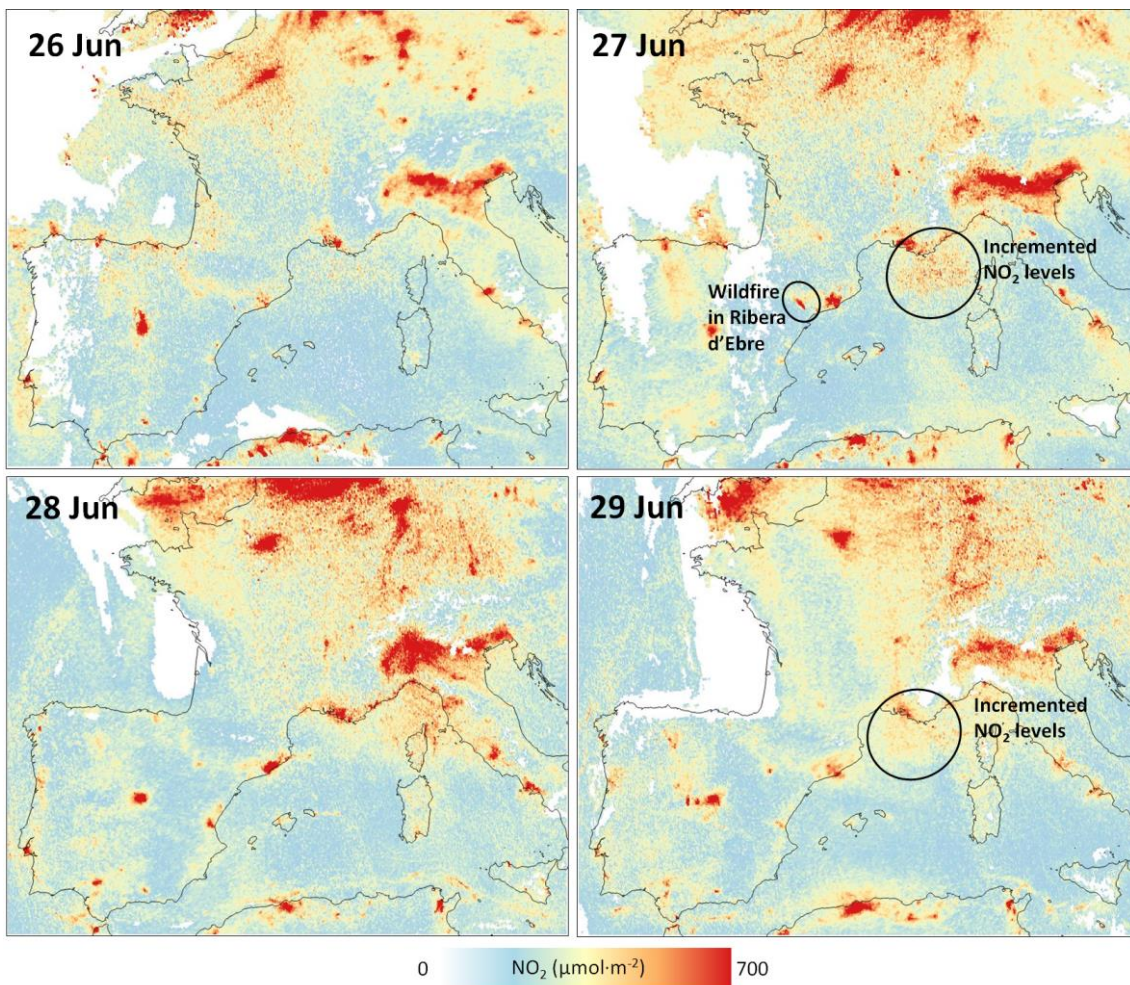
*Figure S3.4. Tropospheric NO₂ concentrations observed by TROPOMI–ESA during the 2019 episode.*
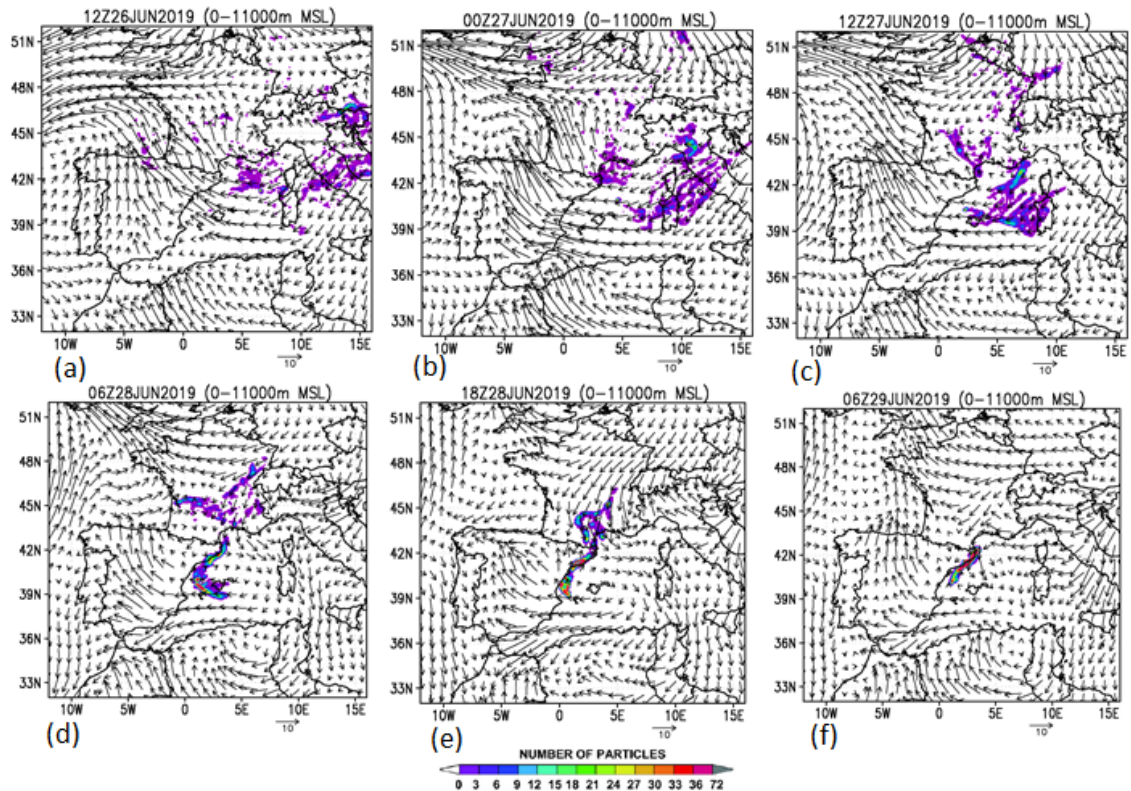
*Figure S3.5. Episode 2019. RAMS/HYPACT back-trajectories of arrival in Barcelona (Fabra) the 29 of June (day of episode). Vectors are average wind from 0–1,000 m above ground level (AGL) (sigma levels), and the shaded areas represent the total number of particles accumulated on the vertical of the site. (a–c) Crossing the Western Mediterranean with east winds, and from central Europe with north winds. (d–f) From the South, following the coast (Mediterranean inputs) with the circulation of the Mediterranean Gyre, and from the North, with a characteristic entry through the Gulf of Lyon, sweeping across southern France (continental Europe contributions).*
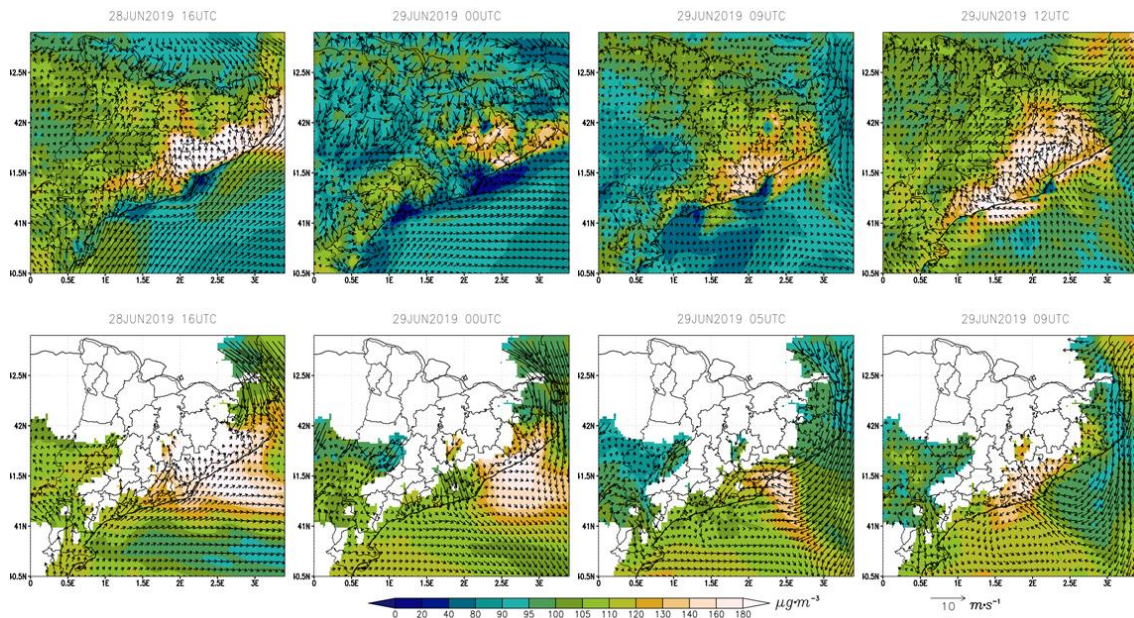
*Figure S3.6. Episode 2019. (Top row) Simulated O₃ concentrations (colour scale) and average wind fields (vectors) at (top row) surface level and at (bottom row) 600 m above ground level.*

## S4. Photochemical model configuration

The model configuration can be found in Torre-Pascual et al. (2023) and the specifics for the simulations in this study are shown below.
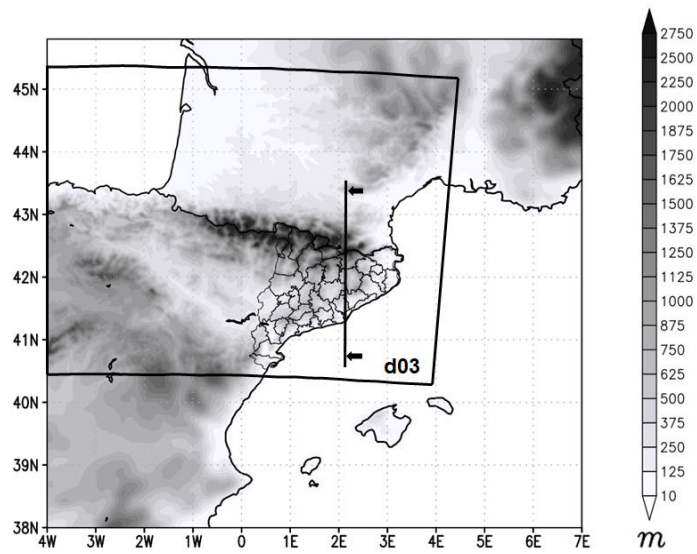
*Figure S4.1. Spatial simulated coverage shown in the manuscript within d02 (9 km) – Iberian Peninsula – and partial view of the domain d03 (3 km) – Northern Iberian Peninsula – on its topographic map. The line shows the extension of the atmospheric cross-section analysed in Barcelona.*

*Table S 4.1. Defined vertical levels for the WRF simulation and correspondence with, CAMx levels.*

| WRF level number | CAMx level number | WRF η level | Approximate height of the CAMx layer interface (m above ground level) |
|---|---|---|---|
| 1 | 1 | 1 | Surface |
| 2 | 2 | 0.9975 | 20 |
| 3 | 3 | 0.9950 | 40 |
| 4 | 4 | 0.9925 | 60 |
| 5 | 5 | 0.9900 | 80 |
| 6 | 6 | 0.9875 | 100 |
| 7 | 7 | 0.9850 | 120 |
| 8 | 8 | 0.9800 | 150 |
| 9 | 9 | 0.9700 | 235 |
| 10 | 10 | 0.9550 | 355 |
| 11 | 11 | 0.9400 | 480 |
| 12 | 12 | 0.9250 | 590 |
| 13 | 13 | 0.9100 | 730 |
| 14 | 14 | 0.8950 | 850 |
| 15 | 15 | 0.8800 | 1,000 |
| 16 | 16 | 0.8650 | 1,100 |
| 17 | 17 | 0.8500 | 1,250 |
| 18 | 18 | 0.8350 | 1,400 |
| 19 | 19 | 0.8200 | 1,500 |
| 20 | 20 | 0.8050 | 1,650 |
| 21 | 21 | 0.7900 | 1,800 |
| 22 | 22 | 0.7750 | 1,900 |
| 23 | 23 | 0.7600 | 2,000 |
| 24 | 24 | 0.7450 | 2,200 |
| 25 | 25 | 0.7300 | 2,400 |
| 26 | 26 | 0.7150 | 2,500 |
| 27 | 27 | 0.7000 | 2,700 |
| 28 | 28 | 0.6850 | 2,800 |
| 29 | 29 | 0.6700 | 2,950 |
| 30 | 30 | 0.6550 | 3,100 |
| 31 | 31 | 0.6400 | 3,300 |
| 32 | 32 | 0.6250 | 3,500 |
| 33 | 33 | 0.6100 | 3,650 |
| 34 | 34 | 0.5950 | 3,800 |
| 35 | 35 | 0.5800 | 4,000 |
| 36 | 36 | 0.5650 | 4,150 |
| 37 | 37 | 0.5500 | 4,300 |
| 38 | 38 | 0.5350 | 4,500 |
| 39 | 39 | 0.5200 | 4,700 |
| 40 | 40 | 0.5000 | 4,900 |
| 41 | 41 | 0.4800 | 5,200 |
| 42 | 42 | 0.4600 | 5,500 |
| 43 | 43 | 0.4400 | 5,750 |
| 44 | 44 | 0.4200 | 6,000 |

*Table S 4.2. Summary of WRF parameterizations.*

| Parameter | Option |
|---|---|
| Shortwave Radiation | MM5 Shortwave radiation scheme (Dudhia, 1989) |
| Longwave Radiation | Rapid Radiative Transfer Model (RRTM) (Mlawer et al., 1997) |
| Surface Model | Noah LSM (Alapaty et al., 2008) |
| Microphysics | WSM6 (Hong & Lim, 2006) |
| PBL | Yonsei University (YSU) (Hong, Noh & Dudhia, 2006) |
| SST | OISST (Reynolds et al., 2007) |

*Table 4.3. Spatial characteristics of the domains used in WRF and CAMx.*

| Domain | Spatial Resolution | WRF Number of grids | CAMx Number of grids |
|---|---|---|---|
| d01 | 27 km × 27 km | 162 ×162 | 160 × 160 |
| d02 | 9 km × 9 km | 195 × 150 | 193 × 148 |
| d03 | 3 km × 3 km | 393 × 186 | 389 × 182 |

# References

Alapaty, K., Niyogi, D., Chen, F., Pyle, P., Chandrasekar, A., and Seaman, N.: Development of the Flux-Adjusting Surface Data Assimilation System for Mesoscale Models, Journal of Applied Meteorology and Climatology, 47(9), 2331-2350, https://doi.org/10.1175/2008JAMC1831.1, 2008.

Dudhia, J.: Numerical Study of Convection Observed during the Winter Monsoon Experiment Using a Mesoscale Two-Dimensional Model, Journal of the Atmospheric Sciences, 46(20), 3077-3107, https://doi.org/10.1175/1520-0469(1989)046<3077:NSOCOD>2.0.CO;2, 1989.

Hong, S. and Lim, J.: The WRF Single-Moment 6-Class Microphysics Scheme (WSM6), Journal of the Korean Meteorological Society, 42, 129-151, 2006.

Hong, S.-Y., Noh, Y., and Dudhia, J.: A New Vertical Diffusion Package with an Explicit Treatment of Entrainment Processes, Monthly Weather Review, 134, 2318-2341, http://dx.doi.org/10.1175/MWR3199.1, 2006.

Mlawer, E. J., Taubman, S. J., Brown, P. D., Iacono, M. J., and Clough, S. A.: Radiative transfer for inhomogeneous atmospheres: RRTM, a validated correlated-k model for the longwave, Journal of Geophysical Research: Atmospheres, 102(D14), 16663-16682, https://doi.org/10.1029/97JD00237, 1997.

Reynolds, R. W., Smith, T. M., Liu, C., Chelton, D. B., Casey, K. S., and Schlax., M. G.: Daily high-resolution-blended analyses for sea surface temperature, Journal of Climate, 20, 5473–5496, http://doi:10.1175/JCLI-D-14-00293.1, 2007.

Torre-Pascual, E., Gangoiti, G., Rodríguez-García, A., Sáez de Cámara, E., Ferreira, J., Gama, C., Gómez, M. C., Zuazo, I., García, J. A., and de Blas, M.: Analysis of an intense $O_3$ pollution episode in the Atlantic Coast of the Iberian Peninsula using photochemical modelling: characterization of transport pathways and accumulation processes, EGUsphere [preprint], https://doi.org/10.5194/egusphere-2023-387, 2023.